Molecular Imaging
Volume 18: 1-11

DOI: 10.1177/1536012118821034
journals.sagepub.com/home/mix
SAGE

Altered Forebrain Functional Connectivity and Neurotransmission in a Kinase-Inactive *Met* Mouse Model of Autism

Shiyu Tang, PhD[1], Elizabeth M. Powell, PhD[2,3], Wenjun Zhu, MS[1], Fu-Sun Lo, MD[2], Reha S. Erzurumlu, PhD[2], and Su Xu, PhD[1]

Abstract

MET, the gene encoding the tyrosine kinase receptor for hepatocyte growth factor, is a susceptibility gene for autism spectrum disorder (ASD). Genetically altered mice with a kinase-inactive *Met* offer a potential model for understanding neural circuit organization changes in autism. Here, we focus on the somatosensory thalamocortical circuitry because distinct somatosensory sensitivity phenotypes accompany ASD, and this system plays a major role in sensorimotor and social behaviors in mice. We employed resting-state functional magnetic resonance imaging and in vivo high-resolution proton MR spectroscopy to examine neuronal connectivity and neurotransmission of wild-type, heterozygous *Met–Emx1*, and fully inactive homozygous *Met–Emx1* mice. *Met–Emx1* brains showed impaired maturation of large-scale somatosensory network connectivity when compared with wild-type controls. Significant sex × genotype interaction in both network features and glutamate/gamma-aminobutyric acid (GABA) balance was observed. Female *Met–Emx1* brains showed significant connectivity and glutamate/GABA balance changes in the somatosensory thalamocortical system when compared with wild-type brains. The glutamate/GABA ratio in the thalamus was correlated with the connectivity between the somatosensory cortex and the thalamus in heterozygous *Met–Emx1* female brains. The findings support the hypothesis that aberrant functioning of the somatosensory thalamocortical system is at the core of the conspicuous somatosensory behavioral phenotypes observed in *Met–Emx1* mice.

Keywords

autism, resting-state functional magnetic resonance imaging, magnetic resonance spectroscopy, brain network, somatosensory thalamocortical system, met null mice, GABA

Introduction

MET (also known as protein product of the c-*MET* proto-oncogene) is a receptor tyrosine kinase, which binds the ligand hepatocyte growth factor (HGF).[1] Decreased *MET* function is associated with an increased risk of autism spectrum disorder (ASD).[2–5] *MET* transcript expression is prominent in the cerebral cortex, hippocampus, and amygdala.[6] The changes in *Met* signaling during development could affect neuronal number as well as the complexity of the neuropil,[7–9] consequently altering the structure or connectivity in the brain and ultimately impacting its function. In a recent neuroimaging study,[10] when children and adolescents with autism-associated promoter variant in *MET* were clustered into homozygous and heterozygous groups, the *MET* risk allele had strong impact across individuals within the heterozygous group. The results suggested that *MET* risk genotype should be taken into account to stratify individuals with ASD. Human neuroimaging studies likely

[1] Department of Diagnostic Radiology and Nuclear Medicine, University of Maryland School of Medicine, Baltimore, MD, USA
[2] Department of Anatomy and Neurobiology, University of Maryland School of Medicine, Baltimore, MD, USA
[3] National Institute on Alcohol Abuse and Alcoholism, National Institutes of Health, Bethesda, MD, USA

Submitted: 06/08/2018. Revised: 13/11/2018. Accepted: 03/12/2018.

Corresponding Authors:
Su Xu, Department of Diagnostic Radiology and Nuclear Medicine, University of Maryland School of Medicine, 22 South Greene Street, Baltimore, MD 21201, USA.
Email: sxu@umm.edu
Reha S. Erzurumlu, Department of Anatomy and Neurobiology, University of Maryland School of Medicine, 20 Penn Street, HSFII, S259, Baltimore, MD 21201, USA.
Email: rerzurumlu@som.umaryland.edu

reflect the effects of multiple different changes at the genetic level, as reflected in the considerable heterogeneity observed between studies.

Impaired somatosensory processing and subsequent associated deficits in motor skills, interpersonal relations, social skills, and communication are well-documented in neurodevelopmental disorders, including ASD.[11] The term "tactile defensiveness" has emerged to depict the tactile hypo- or hypersensitivity of children with ASD. Mouse models offer a particularly useful paradigm to study the tactile sensitivity deficits. Mice rely heavily on tactile discrimination with their whiskers. A large portion of the primary somatosensory cortex is devoted to representation of whiskers by neural modules in a one-to-one and patterned fashion.[12] These neural modules known as "barrels" in the cortex also exist in subcortical structures, such as the sensory thalamus and the trigeminal brainstem, which carry the whisker inputs to the cortex. Thus, the mouse whisker-barrel system is uniquely advantageous to study the development, plasticity, adult organization, and function of the somatosensory system.

Previously, we have used a mouse line in which Met signaling is inactivated specifically in the cerebral cortex and hippocampus of *Met–Emx1* mice. This mouse line was generated using a *Cre-loxP* recombination strategy. Unlike global *Met* null mutants,[13] *Met–Emx1* mice live to adulthood,[14] allowing examination of brain structure during the postnatal and adult periods. As reported in an earlier anatomical magnetic resonance imaging (MRI) study,[15] the rostral cortex, caudal hippocampus, dorsal striatum, thalamus, and corpus callosum were all larger in adult, but not in juvenile, *Met–Emx1* mice relative to wild-type mice. The specificity of the changes suggests that aberrant expansion of the forebrain is consistent with continued axonal and dendritic growth, potentially leading to improper circuit formation and maintenance. In a separate electrophysiological study, we observed an excitatory/inhibitory (E/I) imbalance in somatosensory thalamocortical transmission in an in vitro slice preparation in the same mouse model,[16] consistent with the E/I imbalance theory in autism.[17] Behavioral deficits in *Met–Emx1* mice have been reported as well.[18,19] Given the tactile impairments associated with neurodevelopmental disorders, genetic associations of *MET* with ASD, and our previous data of anatomical differences in structures and electrophysiology, the *Met–Emx1* mouse line was chosen to study altered somatosensory responses at the circuit level in the intact live animal.

We employed in vivo high-resolution proton magnetic resonance spectroscopy (^{1}H-MRS) and resting-state functional magnetic resonance imaging (rsfMRI) to investigate the neurotransmitters (glutamate and gamma-aminobutyric acid [GABA]) and functional connectivity alterations, respectively, within the somatosensory thalamocortical circuitry. The neuroimaging method rsfMRI is used to investigate regional brain interactions when a subject is not performing an explicit task. Resting-state functional MRI signals are thought to arise from spontaneous low-frequency fluctuations in blood oxygen level-dependent (BOLD) signal. The coherence of BOLD signal—also named "functional connectivity"—can be examined using hypothesis-driven seed-based analysis, which is based on the correlation of the resting-state time series of a selected brain region (seed) with the time series of other regions.[20–22] Functional connectivity detects tightly coupled regions in brain baseline functional systems.[23–26] Therefore, rsfMRI can display basic brain functional organization, which reflects the formation and maintenance of neural networks.[27]

In vivo ^{1}H-MRS is a noninvasive spectroscopic technique capable of measuring neurochemical concentrations in specific regions of the central nervous system.[28–30] At high field strength ($\geq$7 T) with a short echo time ($\leq$25 ms), the resolution of coupled peaks, such as the CH_2 from glutamate and glutamine and GABA, can be clearly resolved, suggesting the potential of measuring GABA at 2.30 ppm without the need of spectral *J*-editing.[29,30] The application of in vivo ^{1}H-MRS provides biochemical information on glutamatergic and GABAergic functions without bias introduced from sample preparation. Alterations of correlation between GABA or glutamate and functional connectivity have been reported in mental disorders or following experimental modulation[31–34] but not yet in ASD. Here, we provide correlations between neurotransmitter levels and functional connectivity within the somatosensory thalamocortical circuitry in *Met–Emx1* mice.

Sets of discrete neural elements linked by connections can be considered a network. An analytical technique—graph theory analysis—is helpful in assessing the brain network properties. A network can be defined in graph theory as a set of nodes or vertices and the edges or lines between them can be quantitatively described by various measures (eg, clustering coefficient, local efficiency, small-worldness [SW]) to assess the network features such as integration, segregation, and resilience.[35] This method is used to characterize organization of networks in neuroimaging studies in humans, nonhuman primates, and rats,[36–39] and it has paved the way for increasingly sophisticated investigations of brain connectivity in the study of ASD.[40,41] Recently, modular structure and hub community were detected in the mouse brain using rsfMRI,[42,43] indicating the presence of a well-organized brain network that shares similar features as primates and rats. In addition to seed-based functional connectivity analysis, we performed a graph theory analysis to compare the transgenic mice with homozygous and heterozygous genotype with wild-type mice in topological organization across brain regions.

Methods

Animals

Founder mice, *Met-fx* (#016974; Jackson Laboratory, Bar Harbor, Maine[44]) and *Emx1-Cre* (#005628; Jackson Laboratory), were crossed and maintained on a C57BL/6J background for >30 generations. Mice with a single inactive *Met* allele, *Met-fx/Emx1-Cre*, are denoted as *Met–Emx1* or heterozygous *Met–Emx1*, and those with 2 inactive alleles are denoted as *Met-Met-Emx1* or homozygous *Met–Emx1*. Mice used in these

experiments were adult male and female littermates from mating nonsibling heterozygotes. Wild-type mice included the *Emx1-Cre* allele alone, the *Met-fx* allele alone, and mice lacking any transgenes. In our previous studies, we observed no differences between these groups,[15,16] and therefore, we combined the data from these groups. We imaged 6 groups: wild-type male (n = 12), wild-type female (n = 12), heterozygous *Met–Emx1* male (n = 12), heterozygous *Met–Emx1* female (n = 12), homozygous *Met-Met-Emx1* male (n = 12), and homozygous *Met-Met-Emx1* female (n = 12) mice. All mice were adults, more than 90 days of age. All procedures conformed to the National Institutes of Health Guide for the Care and Use of Laboratory Animals and were approved by the Institutional Animal Care and Use Committee, University of Maryland, Baltimore.

Image Acquisition

We performed all experiments on a Bruker Biospec 7 T 30-cm horizontal bore scanner (Bruker Biospin MRI GmbH, Ettlingen, Germany) equipped with a BGA12S gradient system and interfaced to a Bruker Paravision 5.1 console. A Bruker 72-mm linear-volume coil served as the transmitter and a Bruker ^{1}H 4-element surface coil array served as the receiver. Anesthesia was induced using isoflurane ($\sim$1%) with enriched O_2, which is considered appropriate based on previous evidence in rodent models.[45–47] An MR compatible small-animal monitoring and gating system (SA Instruments, Inc., Stony Brook, New York) monitored the respiration rate and body temperature, which was maintained at 36°C to 37.5°C using a warm water bath circulation.

A 3-slice (axial, mid-sagittal, and coronal) scout image using rapid acquisition with fast low-angle shot localized the mouse brain. A fast shimming procedure (FASTMAP) improved the B_0 homogeneity covering the brain. Anatomic images (repetition time/effective echo time [TR/TE_{eff} = 5000/18.42 ms]) were obtained using a 2-dimensional rapid acquisition with relaxation enhancement sequence covering the entire brain. Imaging was performed over a 1.75-cm field of view (FOV) in the coronal plane with an in-plane resolution of 146 μm using 18 slices at 1-mm thickness.

Resting-state functional MRI was acquired matching the anatomic images using a single shot, spin echo planar imaging sequence (TR/TE = 1000/27.6 ms) with a 1.75-cm FOV and an in-plane resolution of 273 μm^2 using 18 slices at 1-mm thickness. Despite a weaker BOLD signal, spin echo provides much less imaging distortion than gradient echo when imaging mouse brains. Therefore, spin echo imaging was used in this study. Figure 1A shows the raw acquisition EPI images from a female mouse. Six hundred repetitions were taken, resulting in a total scanning time of around 10 minutes for each data set. Two rsfMRI sessions were acquired for each animal. During the rsfMRI experiment, we adjusted the isoflurane anesthesia to 0.75% to 1% and the respiratory rate of the mouse was $\sim$50 breaths/minute without any detectable motion.

High-resolution proton magnetic resonance spectroscopy data were obtained from the right somatosensory cortex (2.5 × 1 × 1.5 mm^3, number of averages = 1000) and the right thalamus (2.0 × 2.5 × 1.5 mm^3, number of averages = 600). Prior to acquiring the spectra, the FASTMAP procedure aided the adjustments of all first- and second-order shims over the voxel of interest. After shimming, a typical water line-width was 10 to 11 Hz (0.033–0.037 ppm). This allowed for good separation of the glutamate (γCH_3 2.35 ppm, αCH 3.75 ppm) and GABA (αCH_2 2.28 ppm, βCH_2 1.89 ppm). A short echo time Point-RESolved Spectroscopy (PRESS) pulse sequence (TR/TE = 2500/10 ms) was used for MRS data acquisition.[48] The unsuppressed water signal from the prescribed voxel was collected as a biochemical concentration reference for each scan. The total in vivo imaging acquisition time was 2.5 hours.

Resting-State Functional MRI Processing

We conducted all rsfMRI image preprocessing and processing using SPM12 (http://www.fil.ion.ucl.ac.uk/spm/) and Analysis of Functional NeuroImages (AFNI) (http://afni.nimh.nih.gov/afni). The processing pipeline included slice-timing correction, motion correction, alignment to a study-specific mouse anatomic template, band-pass filtering, orthogonalization of motion-derived parameters, and smoothing. Specifically, the first 10 and last 50 volumes were excluded from each data set according to the stability of animals and the equipment. Slice-timing correction and motion correction were performed in SPM12 with the ninth slice as the reference slice and second-degree B-spline interpolation as the estimation method. The study-specific mouse anatomical template was created in SPM12 with 2 steps. First, the anatomical image of each mouse was aligned to the anatomical image of a representative mouse with fourth-degree B-spline interpolation. Then, the aligned anatomical images were averaged, yielding the study-specific template. Resting-state functional MRI of each mouse was aligned to the study-specific template with the original anatomic image as the source image in SPM12. Next, the motion-derived parameters were regressed and the data were band-pass filtered (0.01–0.1 Hz) and smoothed (Full width at half maximum [FWHM] = 0.6 mm) with 3dBandpass function in AFNI.

Thirty-seven regions of interest (ROIs) were manually defined based on the standard Paxinos and Watson mouse brain atlas[49] (Figure 1B). For each animal, the regionally averaged BOLD time series was extracted from each ROI, and then these extracted time courses of ROIs were correlated using the Pearson correlation coefficient, producing a 37 × 37 correlation matrix. A separate correlation matrix was generated each session for each mouse. A Fisher transformation yielded the *z*-score association matrices. Two sessions of *z*-score matrices were averaged for graph theory analysis.

Graph Theory Analysis

Graph theory analysis was performed in MATLAB (Ver. R2014a; MathWorks, Inc. Natick, Massachusetts, USA)-based program graph analysis toolbox (https://www.nitrc.org/proj

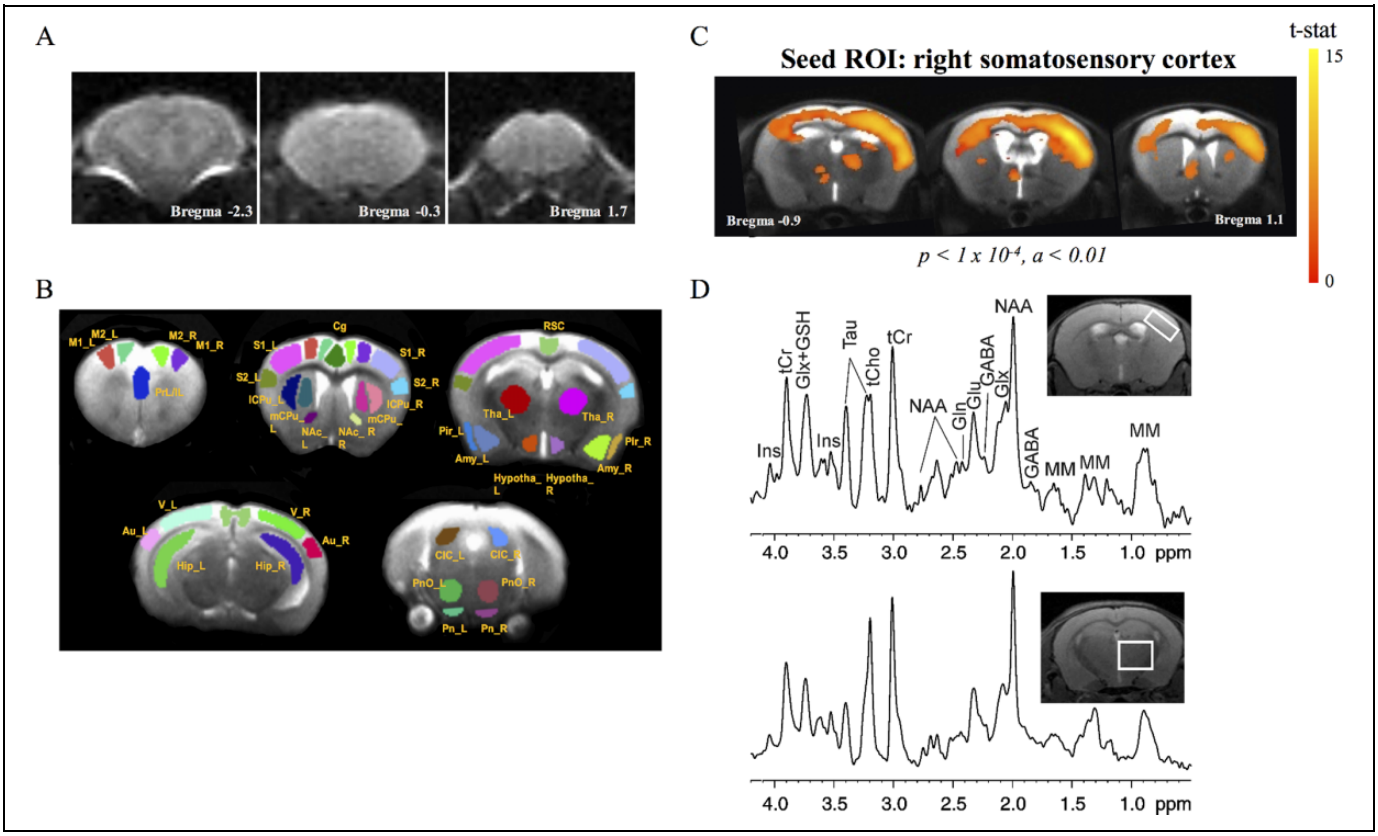

Figure 1. Brain imaging and spectroscopy. Demonstration of the raw EPI images of a female control mouse (A), designation of ROIs for rsfMRI analysis (B), connectivity map of control animals with right-side somatosensory cortex as the seed ROI (C), and representative ^{1}HMRS spectra from somatosensory cortex (top) and thalamus (bottom) (D). Amy indicates amygdala; Au, auditory cortex; Cg, cingulate cortex; CIC, inferior colliculus; GABA, gamma-aminobutyric acid; Gln, glutamine; Glu, glutamate; Glx, glutamate and glutamine; GSH, glutathione; Hip, hippocampus; hypotha, hypothalamus; Ins, *myo*-inositol; lCPu/mCPu, lateral/medial caudate putamen; M1/M2, primary/secondary motor cortex; MM, macromolecules; NAA, *N*-acetyl-aspartate; NAc, nucleus accumbens; Pir, piriform cortex; Pn, pontine nuclei; PnO, rostral pontine reticular nucleus; PrL/IL, prelimbic/infralimbic cortex; RSC, retrosplenial cortex; rsfMRI, resting-state functional magnetic resonance imaging; S1/S2, primary/secondary somatosensory cortex; Tau, taurine; tCho, glycerophosphocholine and phosphocholine; tCr, creatine and phosphocreatine; Tha, thalamus; V, visual cortex; ^{1}HMRS, high-resolution proton magnetic resonance spectroscopy.

ects/gat/). Binary adjacency matrices were derived by thresholding the 37 × 37 association matrices at a range of densities (0.01–0.6). Six global network measures (global efficiency [GEff], local efficiency, SW, Louvian modularity, normalized clustering coefficient, and normalized characteristic path lengths) were calculated at the selected range of densities. To avoid the bias of density selections, a range of densities (0.33–0.4) were used as the target range. The lower boundary was selected at the density when all nodes in the network had at least 1 connection based on the data from the wild-type animals in this study. The upper boundary was set to 0.4 when the averaged SW index was larger than 1.15, based on the range of the SW (eg, 1.1–1.2) used in previous publications.[50–52] Values of the 6 global network measures were calculated for densities from 0.33 to 0.4 with the step of 0.01. The averages were calculated across the target density range and were used for estimating the effect of genotype, sex, and the genotype × sex interaction with 2-way analysis of variance (ANOVA). False discovery rate correction was performed to maintain a 5% type 1 error rate.[53] Corrected *P* values were demonstrated as *Q* values. One-way ANOVA was further performed in males and females on measurements that showed significant genotype × sex interactions. Post hoc analysis was performed with Tukey multiple comparison test. All of the statistical analyses in this study were performed in SPSS Statistics (Version 23.0; SPSS Inc., Chicago, Illinois).

Seed-Based Analysis

For each rsfMRI session, the regionally averaged time course of somatosensory cortex (S1 and S2 combined) was extracted and correlated with the time courses of other voxels in the whole brain to create a correlation map with somatosensory cortex as the seed ROI. For each animal, the correlation map was then transformed to a *z*-score connectivity map with the Fisher transformation, averaged across sessions, and subjected to a 1-way ANOVA (3dANOVA) analysis with males and females separated. 3dFWHMx determined the spatial smoothness of error variance, from which 3dClustSim estimated the required minimum cluster size, maintaining a 5% type 1 error

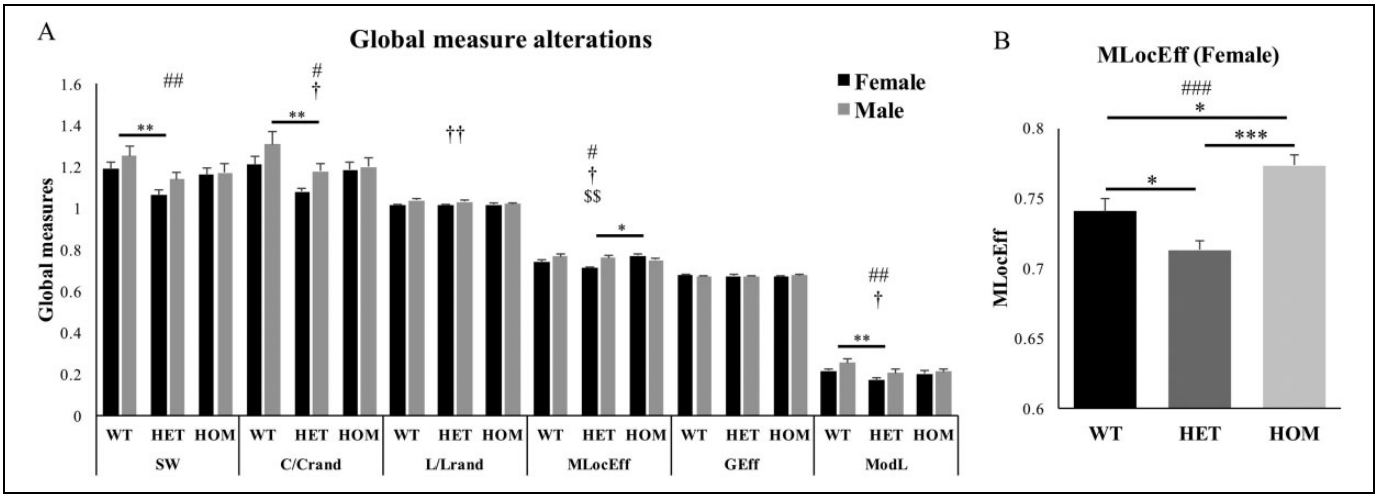

Figure 2. Loss of *Met* allele changed global measurements. Alterations were observed within the densities between 0.33 and 0.4. Two-way ANOVA showed significant effects of genotype or sex and a genotype × sex interaction (A). One-way ANOVA was further performed on MLocEff in both males and females. Only females showed significant genotype effect (B). Values are means ± SEM. $^{\#}P < .05$, $^{\#\#}P < .01$, $^{\#\#\#}P < 0.001$ main genotype effect; $^{\dagger}P < 0.05$, $^{\dagger\dagger}P < 0.01$ main sex effect; $^{\$\$}P < .01$ genotype × sex interaction; $^{*}P < .05$, $^{**}P < .01$, $^{***}P < .001$ between group difference. ANOVA indicates analysis of variance; C/C_{rand}, normalized clustering coefficient; GEff, global efficiency; HET, heterozygous; HOM, homozygous.; L/L_{rand}, normalized characteristic path lengths; MLocEff, local efficiency; ModL, modularity; SEM, standard error of the mean; SW, small-worldness; WT, wild-type.

rate (indicated as α in the Figure 3).[54] The averaged connectivity *z* scores (from the significant clusters in thalamus) were subjected to 2-sample *t* test for quantitative analysis with respect to genotype. Values are reported as mean ± standard error of the mean (SEM). Averaged *z* scores were used in the correlation analysis with neurotransmitter level. The connectivity profile of wild-type animals with right somatosensory cortex as the seed ROI is demonstrated in Figure 1C.

High-resolution proton Magnetic Resonance Spectroscopy Data Analysis

High-resolution proton magnetic resonance spectroscopy data were fitted using the LCModel package.[55] A simulated basis set of model metabolites appropriate for our acquisition parameters was obtained from Stephen Provencher (PhD; LCMODEL Inc., Oakville, ON, Canada; personal communication, November 2012). We based the criteria for selection of the reliable metabolite concentrations on the Cramer-Rao lower bounds (CRLB) with CRLB $\leq 20\%$ for the rodent brain.[56,57] All concentrations were expressed as mean ± SEM. In the current study, the CRLB values for both GABA ($14.23\% \pm 0.56\%$) and glutamate ($4.89\% \pm 0.11\%$) fulfilled the criteria. Figure 1D illustrates representative in vivo high-resolution ^{1}HMRS spectrum from the right somatosensory cortex and thalamus of 1 male wild-type mouse. We analyzed the levels of GABA, glutamate, and the ratio of glutamate to GABA (glutamate/GABA) with 2-way ANOVA to assess the effects of genotype, sex, and genotype × sex interaction. One-way ANOVA was further performed in males and females when significant genotype × sex interaction was observed. Post hoc analysis was performed with Tukey test. The significance level was set at $P < .05$. Since only females demonstrated significant genotype effect in the seed-based analysis, we performed the correlation between functional connectivity (averaged connectivity *z* scores from the significant cluster in thalamus) and neurotransmitter levels only in females with Pearson correlation test within each group.

Data Availability

The data sets generated and analyzed during the current study are available from the corresponding author upon request.

Results

Network Topology Alteration

The average of global network measures in the target density range were significantly different with respect to the genotype effect in 2-way ANOVA (Figure 2A), that is, SW (genotype: $F[2, 66] = 5.046$, $P = .009$, $Q = 0.024$), normalized clustering coefficient (C/C_{rand}; genotype: $F[2, 66] = 4.745$, $P = .012$, $Q = 0.024$; sex: $F[1, 66] = 4.143$, $P = .046$, $Q = 0.069$), and modularity (ModL; genotype: $F[2, 66] = 5.004$, $P = .009$, $Q = 0.024$; sex: $F[1, 66] = 5.353$, $P = .024$, $Q = 0.048$). Post hoc analysis of the genotype effect showed significantly reduced values in heterozygous *Met–Emx1* mice when compared with wild-type animals (SW: $P = .006$; C/C_{rand}: $P = .008$; ModL: $P = .007$) but not in homozygous *Met–Emx1* mice. Significant effect of genotype, sex, and genotype × sex interaction was observed in local efficiency (MLocEff; genotype: $F[2, 66] = 3.828$, $P = .027$, $Q = 0.04$; sex: $F[1, 66] = 6.523$, $P = .013$, $Q = 0.039$; genotype × sex: $F[2, 66] = 7.137$, $P = .002$, $Q = 0.012$). Therefore, 1-way ANOVA was performed to further

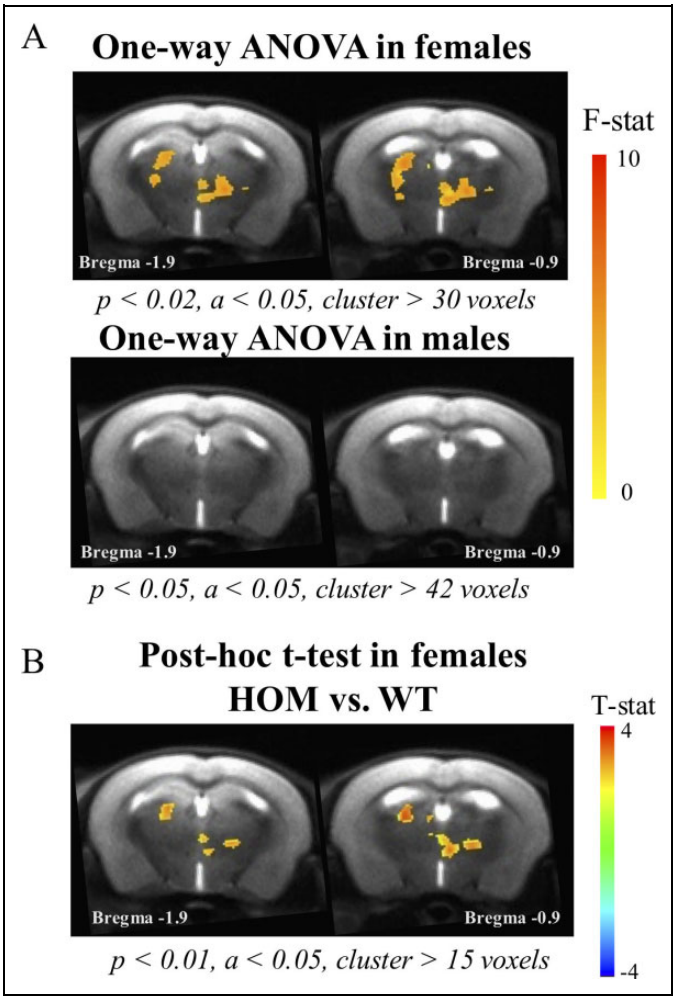

Figure 3. Impaired Met signaling leads to sex-specific differences in functional connectivity. One-way ANOVA shows significant functional connectivity alterations in thalamus with somatosensory cortex (S1 + S2) as the seed ROI in females but not in males (A). Additional post hoc testing demonstrated clusters of voxels in homozygous female mice that were significantly different to control animals (B). α indicates type I error rate; ANOVA, analysis of variance; HET: heterozygous, HOM, homozygous; ROI, region of interest; WT, wild-type.

investigate the effect of genotype on MLocEff in males and females separately. A main effect of genotype was observed in females with $F[2, 33] = 14.678$, $P < .001$ (Figure 2B). MLocEff was significantly increased in female homozygous *Met–Emx1* mice ($P = .016$) and decreased in heterozygous *Met–Emx1* mice ($P = .047$) when compared with wild-type mice. A significant difference between heterozygous and homozygous *Met–Emx1* mice was also observed ($P < .001$) that MLocEff in homozygous *Met–Emx1* mice was significantly higher than in heterozygous *Met–Emx1* mice. Only a main effect of sex was observed in the area under the curve of normalized characteristic path lengths (L/L_{rand}; $F[1, 65] = 8.276$, $P = .005$, $Q = 0.03$). No difference in the effect of genotype, sex, or genotype × sex interaction was observed in the area under the curve of GEff.

Alteration of Somatosensory Thalamocortical Functional Connectivity

The functional connectivity maps of somatosensory cortex (S1 + S2) were subjected to 1-way ANOVA with males and females analyzed separately. Clusters in thalamus with main effect of genotype were only observed in females, $P < .02$ (type 1 error rate, $\alpha < 0.05$), as shown in Figure 3A. In addition, between-group comparison showed increased somatosensory thalamocortical connectivity in female homozygous *Met–Emx1* mice when compared with wild-type female mice, $P < .01$ (type 1 error rate, $\alpha < 0.05$) (Figure 3B). The averaged connectivity z score of clusters with a main effect of genotype significantly increased 189% in female homozygous *Met–Emx1* mice (0.17 ± 0.02) when compared with wild-type females (0.06 ± 0.01), $P < .001$. The z scores were subsequently used for investigation on the correlation between somatosensory thalamocortical functional connectivity and neurotransmitter levels. Heterozygous mice did not differ significantly from the wild-type mice.

Excitatory/Inhibitory Alteration in Met–Emx1 mice

Our previous in vitro electrophysiology study implicated impaired *Met* signaling in decreased GABAergic inhibition and increased E/I ratio.[16] Magnetic resonance spectroscopy tested the hypothesis that *Met–Emx1* mice have an altered E/I balance, as measured by in vivo glutamate and GABA levels. In the right somatosensory cortex (S1 + S2), no significant alteration in glutamate, GABA, or glutamate/GABA ratio was detected (Figure 4A). In the right thalamus, significant genotype × sex interaction was observed in glutamate/GABA ratio (sex: $F[1, 66] = 5.468$, $P = .022$; genotype × sex: $F[2, 66] = 3.990$, $P = .023$; Figure 4B). A 1-way ANOVA was performed with males and females separately to assess the differences among genotypes. Only female mice showed a main effect of genotype, with $F[2, 33] = 6.483$, $P = .004$. Post hoc analysis revealed higher glutamate/GABA ratio in female heterozygous *Met–Emx1* mice when compared with female homozygous *Met–Emx1* mice ($P = .003$). There was a trend toward increased glutamate/GABA ratio in female heterozygous *Met–Emx1* mice when compared with female wild-type mice ($P = .093$; Figure 4B).

Correlation Between Glutamate/GABA Ratio and Functional Connectivity

The averaged connectivity z scores from the cluster in thalamus showing significant effect of genotype were used in the correlation analysis with neurotransmitter levels.

Correlations between thalamic glutamate/GABA ratio and somatosensory thalamocortical functional connectivity were estimated in females, with the 3 genotypic groups analyzed separately (Figure 5). Only a significant negative correlation between somatosensory thalamocortical functional connectivity and thalamic glutamate/GABA ratio was observed in

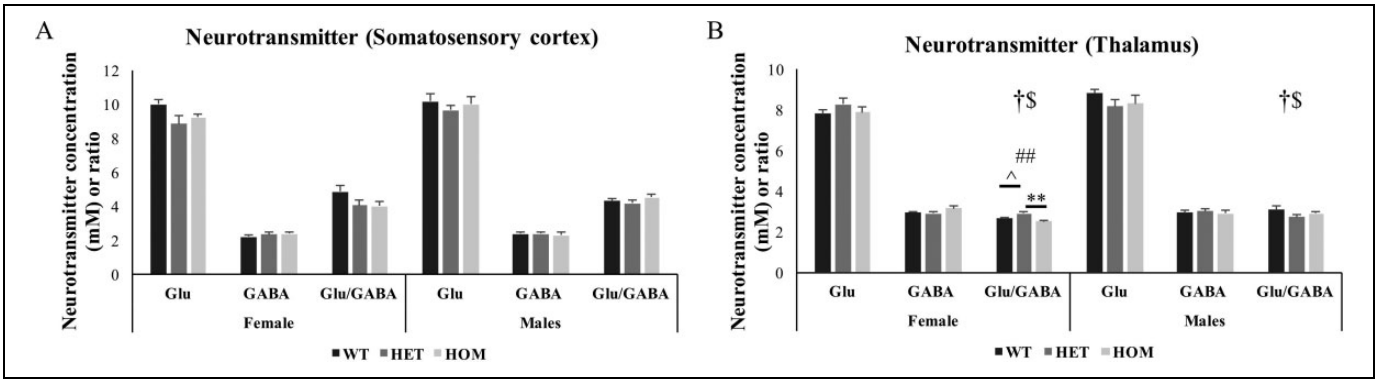

Figure 4. Comparison of glutamate and GABA levels. The concentrations of glutamate and GABA and the glutamate/GABA ratio were measured in somatosensory cortex (A) and thalamus (B). Values are means ± SEM. Two-way ANOVA showed significant effect of sex and genotype × sex interaction of Glu/GABA ratio in thalamus. One-way ANOVA was further performed on measurements with significant genotype × sex interaction in both males and females. Only females showed significant genotype effect on Glu/GABA ratio in thalamus. $^{\#\#}P < .01$ main genotype effect; $^{\dagger}P < .05$ main sex effect; $^{\$}P < .05$ genotype × sex interaction; $^{**}P < .01$ between group difference. $^{\wedge}.05 < P < .1$ trend of between-group difference. ANOVA indicates analysis of variance; GABA, gamma-aminobutyric acid; Glu, glutamate; HET, heterozygous; HOM, homozygous; SEM, standard error of the mean; WT, wild-type.

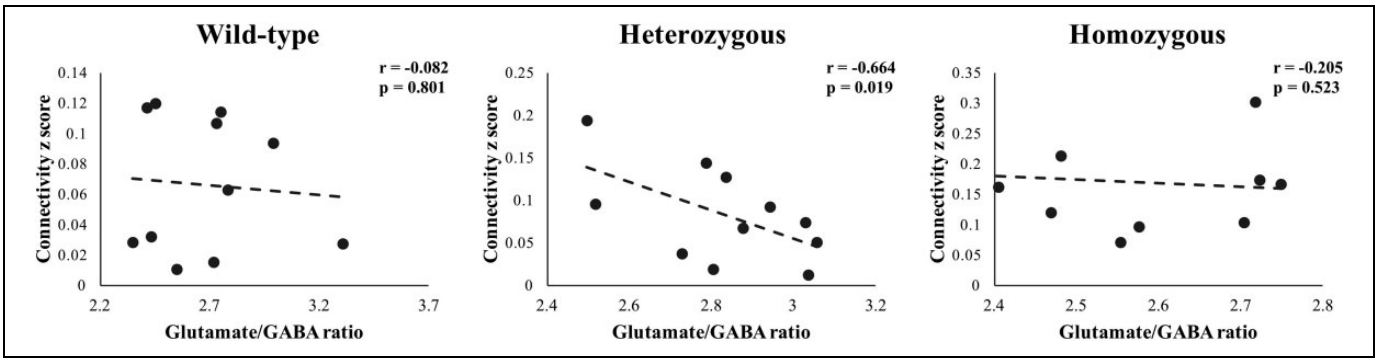

Figure 5. Correlation between thalamic glutamate/GABA ratio and somatosensory thalamocortical functional connectivity. Pearson correlation test revealed significant negative correlation between thalamic glutamate/GABA ratio and functional connectivity between somatosensory cortex and thalamus. GABA indicates gamma-aminobutyric acid.

heterozygous *Met–Emx1* mice ($r = -0.664$, $P = .019$), while this correlation was absent in wild-type and homozygous *Met–Emx1* mice.

Discussion

Our findings reveal several features of altered neural network communication in mice with targeted *Met* receptor inactivation. Decreased SW, normalized clustering coefficient, and modularity in heterozygous *Met–Emx1* mice were observed when compared with wild-type ones. In addition, local efficiency in female mice was significantly increased in homozygous *Met–Emx1* mice and decreased in heterozygous *Met–Emx1* mice when compared with wild-type mice. In female *Met–Emx1* mice, we found (1) a significantly increased functional connectivity between somatosensory cortex and thalamus in homozygous *Met–Emx1* mice when compared with wild-type mice, (2) glutamate/GABA ratio in thalamus is negatively correlated with the somatosensory thalamocortical connectivity in heterozygous *Met–Emx1* mice, and (3) a marginally increased glutamate/GABA ratio in thalamus of heterozygous *Met–Emx1* mice and significantly higher glutamate/GABA ratio in female heterozygous *Met–Emx1* mice when compared with female homozygous *Met–Emx1* mice.

The reduced network modularity, SW, and normalized clustering coefficient in the current study agree with previous studies involving young autism patients.[58,59] Altered clustering coefficient and local efficiency indicated altered brain functional segregation.[35] The features of SW of brain functional networks were formed during typical brain maturational processes when functional connectivity tends to weaken locally and strengthen over longer distances.[60–62] The present results demonstrated that cortical and hippocampal disruptions of HGF-Met signaling during the brain maturational process may impair the maturation of large-scale network community. Hyperconnectivity has been observed in thalamocortical system of individuals with ASD.[63,64] Enhanced somatosensory thalamocortical connectivity in the present study provides

evidence that the disruption of HGF-Met signaling in the neocortex during development can lead to functional deficit in the somatosensory inhibitory system and contribute to the autistic phenotype.

Previous studies noted altered E/I balance in ASD, involving both glutamate and GABA (reviewed by Nelson and Valakh).[17] Our previous in vitro electrophysiology study[16] indicated that the E/I ratio increases due to a dramatic reduction in postsynaptic inhibition, as reflected in decreased amplitude of the spontaneous inhibitory postsynaptic currents in the thalamocortical pathway in *Met–Emx1* mice.[16] Our current study showed that although the absolute concentrations of glutamate and GABA were not altered in *Met–Emx1* mice, the glutamate/GABA ratio showed an increase which provides in vivo evidence to support the E/I imbalance theory in kinase-inactive *Met* mice. Loss of *Met* activity, specifically in interneurons, has been reported to impair cognitive and procedural behaviors.[8] The negative correlation between the glutamate/GABA ratio in the thalamus with the somatosensory thalamocortical connectivity in *Met–Emx1,* but not in wild-type mice, provides a link between the neurotransmission imbalance and thalamocortical system overconnectivity in this model. Future studies will design appropriate behavior tests to investigate whether *Met–Emx1* mice show impaired thalamocortical system behavior, correlated to neurotransmission imbalance and brain functional overconnectivity.

Other novel findings of the current study are the difference between heterozygous and homozygous *Met–Emx1* mice and between males and females. Sex differences, specifically a "male bias" or "female protective effect," have been noticed in previous studies that males are affected more frequently than females.[65,66] Recently, there is an emerging awareness that the sex differences may be due to different phenotypic presentation in females and the failure of detecting autistic females by current diagnostic procedures.[65,67,68] Autism may manifest itself differently, and in some ways more subtly, in females.[69] Recent studies have identified sex-related differences in behavioral characteristics.[70,71] But research to date is yet to define or provide a systematic understanding of the female presentation.[69,72] In this study, male heterozygous *Met–Emx1* mice presented more alterations than male homozygous *Met–Emx1* mice when compared with wild-type mice in network topology, while both female heterozygous and homozygous *Met–Emx1* mice showed network topological alterations and thalamic E/I imbalance. These findings indicate that fully inactive *Met* in the cerebral cortex and hippocampus does not necessarily result in more alterations than single allele inactivation of *Met.* The lack of differences in homozygous *Met–Emx1* mice may be due to early compensation for the complete lack of *Met* Signaling, due to the inactivated allele. Also, the sex bias that males are more prone to autism-associated impairment may not hold true when focusing on a specific genetic basis.

Our results are consistent with some of the observations from individuals with the *Met* susceptibility alleles[10] but not all. The genetic changes are different in each case. In the *Met–Emx1* mice, the Met receptor is inactive, whereas in individuals, the rs1858830 variant is located in a noncoding region and appears to alter *MET* expression. Although the *MET* rs1858830 variant has a strong impact in both heterozygous and homozygous cases, the *Met–Emx1* mice did not show a strong phenotype in the heterozygous group. A possible explanation is that in the *Met–Emx1* mice, *Met* was altered only in the cerebral cortex and hippocampal regions, and the full phenotype may involve subcortical areas and inactivation of *Met* in broader brain areas may generate phenotypes more similar to the human results.

The present study should be viewed with the caveat that anesthetic isoflurane, also a vasodilator, can alter cerebrovascular activity and can have dose-dependent effects on both task-based and resting-state BOLD responses.[46,73] We used the minimum dose of isoflurane (1%) to maintain the immobility of the animals. Imaging with this dose or higher doses has shown preserved brain network activity and network organization in rodents.[42,73,74] Therefore, the functional connectivity observed in this study should represent the intrinsic property of functional brain organization. However, the possibility exists that mice with different genotypes respond differently to isoflurane. To resolve this question, future studies testing cerebral blood flow will be necessary.

In conclusion, our study revealed altered thalamocortical functional connectivity and correlations between neural circuits and neurotransmission in mice with the inactive autism-associated Met tyrosine kinase. The present results provide valuable in vivo evidence to support our hypothesis that aberrant functioning of the somatosensory thalamocortical system is at the core of the conspicuous somatosensory behavioral phenotypes observed in *Met–Emx1* mice and in individuals with ASD. The relative level of glutamate and GABA can play an important role in the functioning of the somatosensory thalamocortical system.

Authors' Note

S.T. acquired, analyzed, and interpreted the data; wrote the manuscript; and assisted with final editorial changes. W.Z. assisted with MR data acquisition. F.L. conducted the animal preparations. R.S.E. and E.M.P. designed the MRI experiment and contributed to the writing of the manuscript and interpretation of the data. S.X. assisted significantly with experimental design, MR data acquisition, data analysis, data interpretation, writing of the manuscript, and assisted with final editorial changes.

Acknowledgments

The authors are grateful to Dr. Rao Gullapalli for contributing to data interpretation. The authors thank Michelle Monroe and Shuxin Zhao for genotyping and breeding the mice.

Declaration of Conflicting Interests

The author(s) declared no potential conflicts of interest with respect to the research, authorship, and/or publication of this article.

Funding

The author(s) disclosed receipt of the following financial support for the research, authorship, and/or publication of this article: This work

was supported by the National Institutes of Health/ National Institutes of Neurological Disorders and Stroke (NS092216).

References

1. Naldini L, Weidner KM, Vigna E, et al. Scatter factor and hepatocyte growth factor are indistinguishable ligands for the MET receptor. *EMBO J*. 1991;10(10):2867–2878.
2. Campbell DB, Sutcliffe JS, Ebert PJ, et al. A genetic variant that disrupts MET transcription is associated with autism. *Proc Natl Acad Sci U S A*. 2006;103(45):16834–16839.
3. Sousa I, Clark TG, Toma C, et al. MET and autism susceptibility: family and case-control studies. *Eur J Hum Genet*. 2009;17(6): 749–758.
4. Jackson PB, Boccuto L, Skinner C, et al. Further evidence that the rs1858830 C variant in the promoter region of the MET gene is associated with autistic disorder. *Autism Res*. 2009;2(4):232–236.
5. Thanseem I, Nakamura K, Miyachi T, et al. Further evidence for the role of MET in autism susceptibility. *Neurosci Res*. 2010; 68(2):137–141.
6. Judson MC, Eagleson KL, Wang L, Levitt P. Evidence of cell-nonautonomous changes in dendrite and dendritic spine morphology in the met-signaling-deficient mouse forebrain. *J Comp Neurol*. 2010;518(21):4463–4478.
7. Martins GJ, Plachez C, Powell EM. Loss of embryonic MET signaling alters profiles of hippocampal interneurons. *Dev Neurosci*. 2007;29(1-2):143–158.
8. Martins GJ, Shahrokh M, Powell EM. Genetic disruption of Met signaling impairs GABAergic striatal development and cognition. *Neuroscience*. 2011;176:199–209.
9. Powell EM, Campbell DB, Stanwood GD, Davis C, Noebels JL, Levitt P. Genetic disruption of cortical interneuron development causes region- and GABA cell type-specific deficits, epilepsy, and behavioral dysfunction. *J Neurosci*. 2003;23(2):622–631.
10. Rudie JD, Hernandez LM, Brown JA, et al. Autism-associated promoter variant in MET impacts functional and structural brain networks. *Neuron*. 2012;75(5):904–915.
11. Cascio CJ. Somatosensory processing in neurodevelopmental disorders. *J Neurodev Disord*. 2010;2(2):62–69.
12. Erzurumlu RS, Gaspar P. Development and critical period plasticity of the barrel cortex. *Eur J Neurosci*. 2012;35(10): 1540–1553.
13. Bladt F, Riethmacher D, Isenmann S, Aguzzi A, Birchmeier C. Essential role for the c-met receptor in the migration of myogenic precursor cells into the limb bud. *Nature*. 1995;376(6543): 768–771.
14. Judson MC, Bergman MY, Campbell DB, Eagleson KL, Levitt P. Dynamic gene and protein expression patterns of the autism-associated met receptor tyrosine kinase in the developing mouse forebrain. *J Comp Neurol*. 2009;513(5):511–531.
15. Smith JM, Xu J, Powell EM. Age dependent forebrain structural changes in mice deficient in the autism associated gene Met tyrosine kinase. *Neuroimage Clin*. 2012;1(1):66–74.
16. Lo FS, Erzurumlu RS, Powell EM. Insulin-Independent GABAA receptor-mediated response in the barrel cortex of mice with impaired met activity. *J Neurosci*. 2016;36(13):3691–3697.
17. Nelson SB, Valakh V. Excitatory/inhibitory balance and circuit homeostasis in autism spectrum disorders. *Neuron*. 2015;87(4): 684–698.
18. Thompson BL, Levitt P. Complete or partial reduction of the Met receptor tyrosine kinase in distinct circuits differentially impacts mouse behavior. *J Neurodev Disord*. 2015;7:35.
19. Smith JM, Powell EM. Mice with impaired met tyrosine kinase signaling demonstrate characteristics relevant to autism. *Autism*. 2012;S1:002.
20. Biswal BB, Van Kylen J, Hyde JS. Simultaneous assessment of flow and BOLD signals in resting-state functional connectivity maps. *NMR Biomed*. 1997;10(4-5):165–170.
21. Cordes D, Haughton VM, Arfanakis K, et al. Mapping functionally related regions of brain with functional connectivity MR imaging. *AJNR Am J Neuroradiol*. 2000;21(9):1636–1644.
22. Jiang T, He Y, Zang Y, Weng X. Modulation of functional connectivity during the resting state and the motor task. *Hum Brain Mapp*. 2004;22(1):63–71.
23. Deco G, Ponce-Alvarez A, Mantini D, Romani GL, Hagmann P, Corbetta M. Resting-state functional connectivity emerges from structurally and dynamically shaped slow linear fluctuations. *J Neurosci*. 2013;33(27):11239–11252.
24. Damoiseaux JS, Rombouts SA, Barkhof F, et al. Consistent resting-state networks across healthy subjects. *Proc Natl Acad Sci U S A*. 2006;103(37):13848–13853.
25. Fox MD, Raichle ME. Spontaneous fluctuations in brain activity observed with functional magnetic resonance imaging. *Nat Rev Neurosci*. 2007;8(9):700–711.
26. Raichle ME. Two views of brain function. *Trends Cogn Sci*. 2010; 14(4):180–190.
27. Guerra-Carrillo B, Mackey AP, Bunge SA. Resting-state fMRI: a window into human brain plasticity. *Neuroscientist*. 2014;20(5): 522–533.
28. Xu S, Zhuo J, Racz J, et al. Early microstructural and metabolic changes following controlled cortical impact injury in rat: a magnetic resonance imaging and spectroscopy study. *J Neurotrauma*. 2011;28(10):2091–2102.
29. Xu S, Gullapalli RP, Frost DO. Olanzapine antipsychotic treatment of adolescent rats causes long term changes in glutamate and GABA levels in the nucleus accumbens. *Schizophr Res*. 2015; 161(2-3):452–457.
30. Xu S, Waddell J, Zhu W, et al. In vivo longitudinal proton magnetic resonance spectroscopy on neonatal hypoxic-ischemic rat brain injury: neuroprotective effects of acetyl-L-carnitine. *Magn Reson Med*. 2015;74(6):1530–1542.
31. Horn DI, Yu C, Steiner J, et al. Glutamatergic and resting-state functional connectivity correlates of severity in major depression – the role of pregenual anterior cingulate cortex and anterior insula. *Front Syst Neurosci*. 2010;4:pii: 33.
32. Hu Y, Chen X, Gu H, Yang Y. Resting-state glutamate and GABA concentrations predict task-induced deactivation in the default mode network. *J Neurosci*. 2013;33(47):18566–18573.
33. Kwon SH, Scheinost D, Lacadie C, et al. GABA, resting-state connectivity and the developing brain. *Neonatology*. 2014; 106(2):149–155.

34. Sampaio-Baptista C, Filippini N, Stagg CJ, Near J, Scholz J, Johansen-Berg H. Changes in functional connectivity and GABA levels with long-term motor learning. *Neuroimage*. 2015;106: 15–20.
35. Rubinov M, Sporns O. Complex network measures of brain connectivity: uses and interpretations. *Neuroimage*. 2010;52(3): 1059–1069.
36. Bressler SL, Menon V. Large-scale brain networks in cognition: emerging methods and principles. *Trends Cogn Sci*. 2010;14(6): 277–290.
37. Sporns O. From simple graphs to the connectome: networks in neuroimaging. *Neuroimage*. 2012;62(2):881–886.
38. Telesford QK, Laurienti PJ, Friedman DP, Kraft RA, Daunais JB. The effects of alcohol on the nonhuman primate brain: a network science approach to neuroimaging. *Alcohol Clin Exp Res*. 2013; 37(11):1891–1900.
39. van den Heuvel MP, Scholtens LH, de Reus MA. Topological organization of connectivity strength in the rat connectome. *Brain Struct Funct*. 2016;221(3):1719–1736.
40. Verhoeven JS, De Cock P, Lagae L, Sunaert S. Neuroimaging of autism. *Neuroradiology*. 2010;52(1):3–14.
41. Kennedy DP, Adolphs R. The social brain in psychiatric and neurological disorders. *Trends Cogn Sci*. 2012;16(11):559–572.
42. Bardella G, Bifone A, Gabrielli A, Gozzi A, Squartini T. Hierarchical organization of functional connectivity in the mouse brain: a complex network approach. *Sci Rep*. 2016;6:32060.
43. Liska A, Galbusera A, Schwarz AJ, Gozzi A. Functional connectivity hubs of the mouse brain. *Neuroimage*. 2015;115:281–291.
44. Huh CG, Factor VM, Sanchez A, Uchida K, Conner EA, Thorgeirsson SS. Hepatocyte growth factor/c-met signaling pathway is required for efficient liver regeneration and repair. *Proc Natl Acad Sci U S A*. 2004;101(13):4477–4482.
45. Ferron JF, Kroeger D, Chever O, Amzica F. Cortical inhibition during burst suppression induced with isoflurane anesthesia. *J Neurosci*. 2009;29(31):9850–9860.
46. Liu X, Zhu XH, Zhang Y, Chen W. The change of functional connectivity specificity in rats under various anesthesia levels and its neural origin. *Brain Topogr*. 2013;26(3):363–377.
47. DeSimone JC, Pappas SS, Febo M, et al. Forebrain knock-out of torsinA reduces striatal free-water and impairs whole-brain functional connectivity in a symptomatic mouse model of DYT1 dystonia. *Neurobiol Dis*. 2017;106:124–132.
48. Xu S, Ji Y, Chen X, Yang Y, Gullapalli RP, Masri R. In vivo high-resolution localized (1) H MR spectroscopy in the awake rat brain at 7 T. *Magn Reson Med*. 2013;69(4):937–943.
49. Paxinos G, Franklin K. *The Mouse Brain in Stereotaxic Coordinates*. 4th ed. Cambridge, MA: Academic Press; 2012.
50. Bernhardt BC, Chen Z, He Y, Evans AC, Bernasconi N. Graph-theoretical analysis reveals disrupted small-world organization of cortical thickness correlation networks in temporal lobe epilepsy. *Cereb Cortex*. 2011;21(9):2147–2157.
51. Lu FM, Zhou JS, Zhang J, Wang XP, Yuan Z. Disrupted small-world brain network topology in pure conduct disorder. *Oncotarget*. 2017;8(39):65506–65524.
52. Smit DJ, Stam CJ, Posthuma D, Boomsma DI, de Geus EJ. Heritability of "small-world" networks in the brain: a graph theoretical analysis of resting-state EEG functional connectivity. *Hum Brain Mapp*. 2008;29(12):1368–1378.
53. Benjamini Y, Hochberg Y. Controlling the false discovery rate: a practical and powerful approach to multiple testing. *J R Stat Soc*. 1995;57(1):289–300.
54. Bennett CM, Wolford GL, Miller MB. The principled control of false positives in neuroimaging. *Soc Cogn Affect Neurosci*. 2009; 4(4):4174–4122.
55. Provencher SW. Automatic quantitation of localized in vivo 1 H spectra with LCModel. *NMR Biomed*. 2001;14(4):260–264.
56. Morgan JJ, Kleven GA, Tulbert CD, Olson J, Horita DA, Ronca AE. Longitudinal 1 H MRS of rat forebrain from infancy to adulthood reveals adolescence as a distinctive phase of neurometabolite development. *NMR Biomed*. 2013;26(6):683–691.
57. Harris JL, Yeh HW, Choi IY, et al. Altered neurochemical profile after traumatic brain injury: (1)H-MRS biomarkers of pathological mechanisms. *J Cereb Blood Flow Metab*. 2012;32(12): 2122–2134.
58. Shi F, Wang L, Peng Z, Wee CY, Shen D. Altered modular organization of structural cortical networks in children with autism. *PLoS One*. 2013;8(5):e63131.
59. Barttfeld P, Amoruso L, Ais J, et al. Organization of brain networks governed by long-range connections index autistic traits in the general population. *J Neurodev Disord*. 2013;5(1):16.
60. Fair DA, Cohen AL, Power JD, et al. Functional brain networks develop from a "local to distributed" organization. *PLoS Comput Biol*. 2009;5(5):e1000381.
61. Yap PT, Fan Y, Chen Y, Gilmore JH, Lin W, Shen D. Development trends of white matter connectivity in the first years of life. *PLoS One*. 2011;6(9):e24678.
62. Hagmann P, Sporns O, Madan N, et al. White matter maturation reshapes structural connectivity in the late developing human brain. *Proc Natl Acad Sci U S A*. 2010;107(44): 19067–19072.
63. Nair A, Carper RA, Abbott AE, et al. Regional specificity of aberrant thalamocortical connectivity in autism. *Hum Brain Mapp*. 2015;36(11):4497–4511.
64. Woodward ND, Giraldo-Chica M, Rogers B, Cascio CJ. Thalamocortical dysconnectivity in autism spectrum disorder: an analysis of the Autism brain imaging data exchange. *Biol Psychiatry Cogn Neurosci Neuroimaging*. 2017;2(1):76–84.
65. Werling DM, Geschwind DH. Sex differences in autism spectrum disorders. *Curr Opin Neurol*. 2013;26(2):146–153.
66. Werling DM, Geschwind DH. Understanding sex bias in autism spectrum disorder. *Proc Natl Acad Sci U S A*. 2013;110(13): 4868–4869.
67. Ratto AB, Kenworthy L, Yerys BE, et al. What about the girls? Sex-based differences in Autistic traits and adaptive skills. *J Autism Dev Disord*. 2018;48(5): 1698–1711.
68. Ormond S, Brownlow C, Garnett MS, Rynkiewicz A, Attwood T. Profiling Autism symptomatology: an exploration of the Q-ASC parental report scale in capturing sex differences in Autism. *J Autism Dev Disord*. 2018;48(2): 389–403.
69. Dworzynski K, Ronald A, Bolton P, Happe F. How different are girls and boys above and below the diagnostic threshold for

autism spectrum disorders? *J Am Acad Child Adolesc Psychiatry*. 2012;51(8):788–797.

70. Kopp S, Gillberg C. The Autism Spectrum Screening Questionnaire (ASSQ)-Revised Extended Version (ASSQ-REV): an instrument for better capturing the autism phenotype in girls? A preliminary study involving 191 clinical cases and community controls. *Res Dev Disabil*. 2011;32(6):2875–2888.
71. White EI, Wallace GL, Bascom J, et al. Sex differences in parent-reported executive functioning and adaptive behavior in children and young adults with autism spectrum disorder. *Autism Res*. 2017;10(10):1653–1662.
72. Lai MC, Lombardo MV, Auyeung B, Chakrabarti B, Baron-Cohen S. Sex/gender differences and autism: setting the scene for future research. *J Am Acad Child Adolesc Psychiatry*. 2015;54(1): 11–24.
73. Masamoto K, Fukuda M, Vazquez A, Kim SG. Dose-dependent effect of isoflurane on neurovascular coupling in rat cerebral cortex. *Eur J Neurosci*. 2009;30(2):242–250.
74. Hutchison RM, Mirsattari SM, Jones CK, Gati JS, Leung LS. Functional networks in the anesthetized rat brain revealed by independent component analysis of resting-state FMRI. *J Neurophysiol*. 2010;103(6):3398–3406.